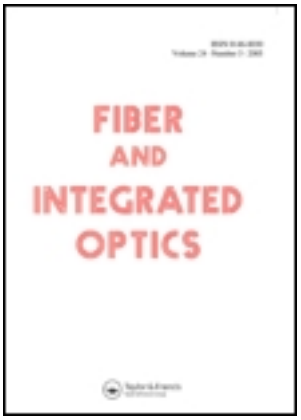

Fiber and Integrated Optics
Publication details, including instructions for authors and subscription information:
http://www.tandfonline.com/loi/ufio20

Polarization-Dependent Mode Analyzer and Controlled-Z Gate in Ti:$LiNbO_3$ Quantum Photonic Circuits

Masoomeh Taherkhani [a] & Shahram Mohammad Nejad [a]
[a] Nanoptronics Research Center, School of Electrical Engineering, Iran University of Science and Technology, Tehran, Iran
Version of record first published: 10 Dec 2012.

To cite this article: Masoomeh Taherkhani & Shahram Mohammad Nejad (2012): Polarization-Dependent Mode Analyzer and Controlled-Z Gate in Ti:$LiNbO_3$ Quantum Photonic Circuits, Fiber and Integrated Optics, 31:6, 355-368

To link to this article: http://dx.doi.org/10.1080/01468030.2012.743808

Fiber and Integrated Optics, 31:355–368, 2012

ISSN: 0146-8030 print/1096-4681 online
DOI: 10.1080/01468030.2012.743808

Taylor & Francis
Taylor & Francis Group

Polarization-Dependent Mode Analyzer and Controlled-Z Gate in Ti:$LiNbO_3$ Quantum Photonic Circuits

MASOOMEH TAHERKHANI[1] and
SHAHRAM MOHAMMAD NEJAD[1]

[1]Nanoptronics Research Center, School of Electrical Engineering, Iran University of Science and Technology, Tehran, Iran

Abstract *On-chip integrated photonic circuits are crucial for further progress toward quantum technologies and in the science of quantum optics. The quantum controlled-Z gate is an example of the maximally entangling gate, which is universal for quantum computing when coupled with single-qubit gates. This article demonstrates a deterministic controlled-Z photonic quantum gate based on titanium in-diffused channel waveguides in which polarization and modal degrees of freedom of a single photon are used for encoding the control and target qubits, respectively.*

Keywords polarization-dependent mode analyzer, quantum controlled-Z gate, quantum photonic circuits

1. Introduction

Presently, information processing is commonly implemented using quantities such as charges, voltages, or currents in electronic devices that operate on the basis of classical physics. Quantum information processing (QIP), instead, employs the laws of quantum mechanics in data storage, processing, and transmission, promising exponential improvement and new functionality for particular tasks in computation, metrology, lithography, and communication [1–6]. Integrated photonic circuits are crucial for further progress toward quantum technologie. Achieving desired scalability, stability, and miniaturization in optical schemes consisting of many elements requires the introduction of waveguide technology [5].

Lithium niobate ($LiNbO_3$) is one of the most attractive materials for quantum integrated circuits. $LiNbO_3$ quantum photonic circuits have the distinct advantage of permitting the generation, transmission, and processing of photons, all achieved on a single chip [7–9]. Moreover, $LiNbO_3$ also has other important advantages, including:

(1) its properties are well understood [7, 10, 11];
(2) it allows the fabrication of low-loss (<0.2 dB/cm) planar and channel waveguides by titanium indiffusion or proton exchange [12];

Received 1 July 2012; accepted 13 August 2012.
Address correspondence to Miss Masoomeh Taherkhani, Nanoptronics Research Center, School of Electrical Engineering, Iran University of Science and Technology (IUST), Narmak, Tehran 16844, Iran. E-mail: m_taherkhani@iust.ac.ir

(3) it exhibits an electro-optic (EO) effect that can modify the refractive index at rates up to tens of GHz and is polarization sensitive [10];
(4) consistency between simulation and experimental measurements has been demonstrated in a whole host of configurations [7]; and
(5) periodic polling of the second-order non-linear optical coefficient is straightforward so that phase-matched parametric interactions, such as spontaneous parametric down conversion (SPDC) and the generation of entangled-photon pairs, can readily be achieved [11, 13].

These attributes have led to the current interest in the use of $LiNbO_3$ in the rapidly advancing field of quantum photonics [5, 7].

All arbitrary quantum computation operations can be performed by one-qubit and any two-qubit gates [14]. Conceptually, the simplest two-qubit gate is the controlled-Z (CZ) gate, which is considered to be one of the most fundamental quantum gates [15]. Recently, with the emergence of one-way quantum computation [16], interest in the realization of the optical CZ gate has increased greatly, and much effort has been devoted to the realization of such a gate in many physical systems, especially in optical systems [17]. However, an integrated photonic quantum CZ gate, which is needed for further advancement on the way to quantum computation technologies, has not been reported so far.

This article is organized as follows. Section 2 describes the structure and properties of Ti:$LiNbO_3$-diffused channel waveguides and the coupling of modes between two adjacent waveguides. Section 3 briefly reviews some basic concepts of quantum computation. Section 4 describes a polarization-dependent mode analyzer, which separates the even and odd components of the TE-polarization incoming state into two separate spatial paths while the TM-polarization even and odd modes remain unchanged. Section 5 reports, for the first time, a deterministic integrated Ti:$LiNbO_3$ photonic quantum CZ gate in which the polarization and mode number of a single photon serve as the control and target qubits, respectively.

2. Diffused Channel Ti:$LiNbO_3$ Waveguides

$LiNbO_3$ is used as a wafer material, and Ti:$LiNbO_3$ is used for waveguides. To form a waveguide, a stripe of titanium is deposited on the $LiNbO_3$ substrate (see Figure 1). For a given stripe width, identified with waveguide width w, the amount of titanium is characterized by the stripe thickness δ before diffusion [18]. The titanium lithium niobate sample is heated for a few hours at temperatures that range from hundreds to 1,000°C.

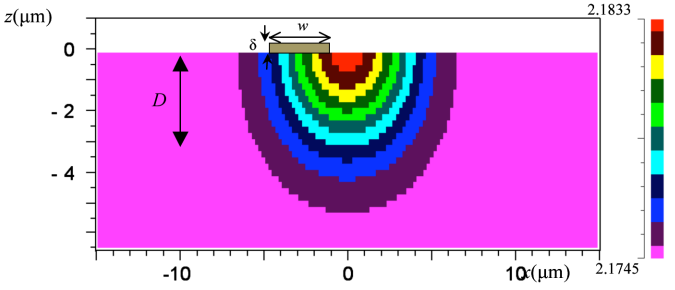

Figure 1. Simulated distribution of refractive index in Ti:$LiNbO_3$ channel waveguide; $D = 3$ μm, $\delta = 50$ nm. (color figure available online)

The titanium ions penetrate the host substrate and form a graded index waveguide. The graded waveguide has a bell-shaped refractive index distribution in the lateral and in-depth directions. The index distribution can be characterized phenomenologically by diffusion lengths or, as an alternative, by diffusion constants, diffusion temperature, and a diffusion temperature coefficient [18].

$LiNbO_3$ is a uniaxial crystal in which one special direction of symmetry, called the optic axis (e.g., the z-axis), exists. The plane containing the optic axis and the wave vector of the light wave is termed as the principal plane. The light beam whose polarization is normal to the principal plane (or TE-polarized light) experiences the ordinary refractive index n_o, while the beam polarized in the principal plane (or TM-polarized light) experiences the extraordinary refractive index n_e. The refractive index of TE-polarized light does not depend on the propagation direction, whereas for the TM-polarized light, it does; $n_e = n_e(\theta)$, where θ is the angle between the optic axis and the wave vector of the light [10].

Here, a thin film of titanium (Ti) was used, with thickness $\delta = 50$ nm and width w, for diffusing into a z-cut, y-propagating $LiNbO_3$ crystal. The diffusion length D is taken to be the same in the two transverse directions: $D = 3\ \mu$m (see Figure 1). The TM mode polarized in the z-direction (along the optic axis) sees the extraordinary refractive index n_e whereas the TE mode polarized in the x-direction sees the ordinary refractive index n_o. The ordinary and extraordinary refractive indices can be calculated by making use of the Sellmeier equations [10, 19, 20]. Applying a steady electric field to this structure in the z-direction (along the optic axis) changes the ordinary and extraordinary refractive indices of this uniaxial material as follows [10]:

$$n_o(E) \approx n_o - \frac{1}{2}n_o^3 r_{13} V/d, \qquad n_e(E) \approx n_e - \frac{1}{2}n_e^3 r_{33} V/d, \tag{1}$$

where V is the applied voltage, d is the separation between the electrodes, and r_{13} and r_{33} are the tensor elements of the Pockels coefficient.

2.1. Mode Coupling Between Adjacent Waveguides

According to coupled-mode theory, the set of equations, which can be used to analyze transferred energy from one lossless and single-mode waveguide to another when the guiding structures are brought into proximity, are [10]

$$\begin{aligned} a_1(y) &= A(y)a_1(0) - jB(y)a_2(0), \\ a_2(y) &= -jB^*(y)a_1(0) + B^*(y)a_2(0), \end{aligned} \tag{2}$$

where $a_1(y)$ and $a_2(y)$ are the amplitudes of guided modes in two waveguides, and

$$\begin{aligned} A(y) &= \exp\left(j\frac{\Delta\beta y}{2}\right)\left(\cos\gamma y - j\frac{\Delta\beta}{2\gamma}\sin\gamma y\right), \\ B(y) &= \frac{\kappa}{\gamma}\exp\left(j\frac{\Delta\beta y}{2}\right)\sin\gamma y; \end{aligned} \tag{3}$$

here, $\Delta\beta$ is the phase mismatch per unit length between two coupled modes; y is the coupling interaction length; κ is the coupling coefficient, which depends on the widths

of the waveguides and their separation as well as on the mode profiles; $\gamma^2 = \kappa^2 + \frac{1}{4}\Delta\beta^2$; and the symbol * presents complex conjugation [10].

Equation (2) can also be described by unitary matrix **T**, which takes the form [10]

$$\mathbf{T} = \begin{pmatrix} A & -jB \\ -jB^* & A^* \end{pmatrix}. \tag{4}$$

For perfect phase matching between the coupled modes, i.e., for $\Delta\beta = 0$, and an interaction coupling length $L = q\pi/2\kappa$, where q is an odd positive integer, the coupling matrix **T** reduces to

$$\mathbf{T} = \exp\left(\frac{jq\pi}{2}\right)\begin{pmatrix} 0 & -1 \\ -1 & 0 \end{pmatrix}, \tag{5}$$

indicating that the modes are flipped. Applying this operation twice serves to double flip the vector, thereby reproducing the input but with a phase shift twice that of $q\pi/2$ [7].

If it is assumed that no light enters waveguide 2 so that $a_2(0) = 0$, then optical powers $P_1(z) \propto |a_1(z)|^2$ and $P_2(z)) \propto |a_2(z)|^2$ with respect to Eqs. (2) and (3) can be written as [10]:

$$\begin{aligned} P_1(y) &= P_1(0)\left(\cos^2\gamma y + \left(\frac{\Delta\beta}{2\gamma}\right)^2 \sin^2\gamma y\right), \\ P_2(y) &= P_1(0)\frac{|\kappa|^2}{\gamma^2}\sin^2\gamma y. \end{aligned} \tag{6}$$

Thus, power is exchanged periodically between two waveguides; the period is π/γ.

When the waveguides are identical, i.e., $n_1 = n_2$, $\beta_1 = \beta_2$, and $\Delta\beta = 0$, the equations then simplify to

$$\begin{aligned} P_1(y) &= P_1(0)\cos^2\kappa y, \\ P_2(y) &= P_1(0)\sin^2\kappa y. \end{aligned} \tag{7}$$

The exchange of power between the waveguides can then be completed. At the interaction length $y = q\pi/2\kappa$, the odd integer multiple of the coupling length, the power is transferred completely from waveguide 1 into waveguide 2. The application of a voltage to the EO modulator introduces a phase mismatch ($\Delta\beta \neq 0$) between the two interacting modes, which results in partial, rather than full, optical power transfer [10].

The matrix described in Eq. (4) is not adequate for describing the coupling between two-mode waveguides (TMWs), which is of interest in this article; in this case, a 4×4 matrix is required. However, for the particular cases considered here, the coupling between the two waveguides is such that only a single mode in each waveguide participates; this is because the phase-matching conditions between the interacting modes are either satisfied—or not satisfied. As an example for identical waveguides, similar modes couple whereas dissimilar modes fail to couple as a result of the large phase mismatch. So the general matrix described in Eq. (4) reduces to submatrices of size 2×2, each characterizing the coupling between a pair of modes [7, 10].

3. Qubits and Quantum Computation

Classical information is in binary format, stored as 0 and 1, and the computation operations are performed on these binary bits. At the heart of quantum computation lies the ability to represent information as qubits, superposition states of both 0 and 1. Before measurement, the qubit can be considered to be in two states at the same time. Upon measurement, the superposition state collapses into one of the base states (being 0 or 1 in this case), with a probability defined by the superposition state. For quantum systems with many qubits, the size of the superposition state increases with the number of qubits such that a system with n qubits can be considered as being in $2n$ states simultaneously. This is the key to the exponential computational power of a quantum computer [21].

Over the last few years, single particles of light photons have emerged as one of the several leading approaches for realizing qubits. Any of several degrees of freedom of a single photon, such as polarization, spatial parity, or the mode number of a single photon confined to a TMW, can be used for encoding qubit [7–9]. Polarization is an intrinsically binary basis. In this case, an arbitrary state of a single qubit can be expressed as $|\Psi\rangle = \alpha_1|H\rangle + \alpha_2|V\rangle$, where a horizontal ($H$) photon represents a logical "0" and a vertical (V) photon represents a logical "1": $|0\rangle \equiv |H\rangle$ and $|1\rangle \equiv |V\rangle$. α_1 and α_2 are their weights, respectively. The spatial modes of a photon in a TMW, one of which is even and the other odd, are also binary and can therefore be used to represent a qubit. Similar to a polarization qubit, $|\Psi\rangle = \beta_1|e\rangle + \beta_2|o\rangle$ can be used for representing a modal qubit, where $|e\rangle$ and $|o\rangle$ represent the even and odd basis states and β_1 and β_2 are their weights, respectively. Modal qubits are particularly suited to photonic quantum circuits, since they can both be generated and easily transformed on-chip. The modal space of a TMW is therefore an appealing choice for representing qubits in quantum photonic circuits.

A universal quantum computer could be implemented by using only arbitrary one-qubit operations and any two-qubit gates [14], the same way that classical computers can be constructed from a very limited gate set. A two-qubit quantum logic gate requires qubits to interact with one another. A set of one-qubit gates, which turns out to be of fundamental importance in quantum computation, is known as Pauli gates [21]. There are three Pauli gates, denoted by X, Y, and Z. The Pauli operators are both Hermitian and unitary. These one-qubit gates act on the superposition state $|\Psi\rangle = \alpha|0\rangle + \beta|1\rangle$ in the following way [21]:

$$X(|\Psi\rangle) = \alpha|1\rangle + \beta|0\rangle, \qquad (|\Psi\rangle) = -i\alpha|1\rangle + i\beta|0\rangle, \qquad Z(|\Psi\rangle) = \alpha|0\rangle - \beta|1\rangle. \quad (8)$$

Two-qubit (or controlled unitary) gates work in a similar fashion, using a control qubit to determine whether or not a specified unitary action is applied to a target qubit. One of the most important two-qubit gates, the CZ gate, acts on the logical basis $|00\rangle$, $|01\rangle$, $|10\rangle$, and $|10\rangle$ as follows [21]:

$$|00\rangle \to |00\rangle, \qquad |01\rangle \to |01\rangle, \qquad |10\rangle \to |10\rangle, \qquad |11\rangle \to -|11\rangle. \quad (9)$$

If the control qubit (first qubit) is $|0\rangle$, then nothing happens to the target qubit (second qubit; but when the control qubit is $|1\rangle$, it produces a π phase shift on the target qubit $|1\rangle$. CZ is a maximally entangling gate, which, when coupled with single-qubit rotations, is universal for quantum computing [22].

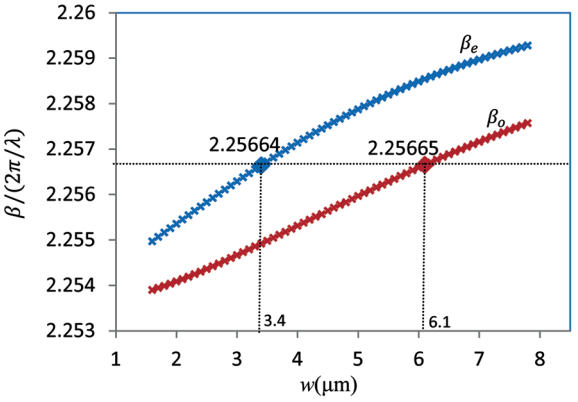

Figure 2. Normalized propagation constants of TE polarization even (β_e) and odd (β_o) modes for diffused channel Ti:$LiNbO_3$ waveguides as a function of the waveguide width w. (color figure available online)

4. Polarization-Dependent Mode Analyzer

Since Ti:$LiNbO_3$ waveguides have different refractive indices values n, dependent upon the polarization of the input light, a mode analyzer can be designed that separates the even and odd components of an incoming state into two separate spatial paths according to its polarization. The even ($m = 0$) and odd ($m = 1$) modes of a Ti:$LiNbO_3$ waveguide are characterized by different propagation constants: β_e and β_o, respectively. Figures 2 and 3 show the behavior of the normalized propagation constants β_e and β_o as a function of the waveguide width w for TE and TM polarization, respectively (at a wavelength of $\lambda = 0.812\ \mu$m). The horizontal dotted line, crossing the two curves, represents the phase-matching condition for an even and odd mode in two waveguides of different widths.

The operating principle of the designed polarization-dependent mode analyzer, shown in Figure 4, is based on the selective coupling between two adjacent waveguides of different widths w_1 and w_2. A waveguide with appropriate width w_2, length L_2, and

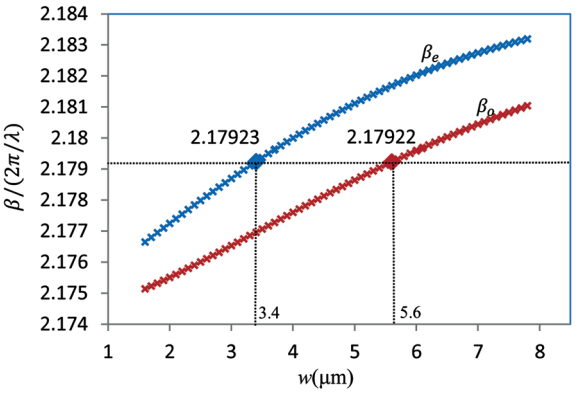

Figure 3. Normalized propagation constants of TM polarization even (β_e) and odd (β_o) modes for diffused channel Ti:$LiNbO_3$ waveguides as a function of the waveguide width w. (color figure available online)

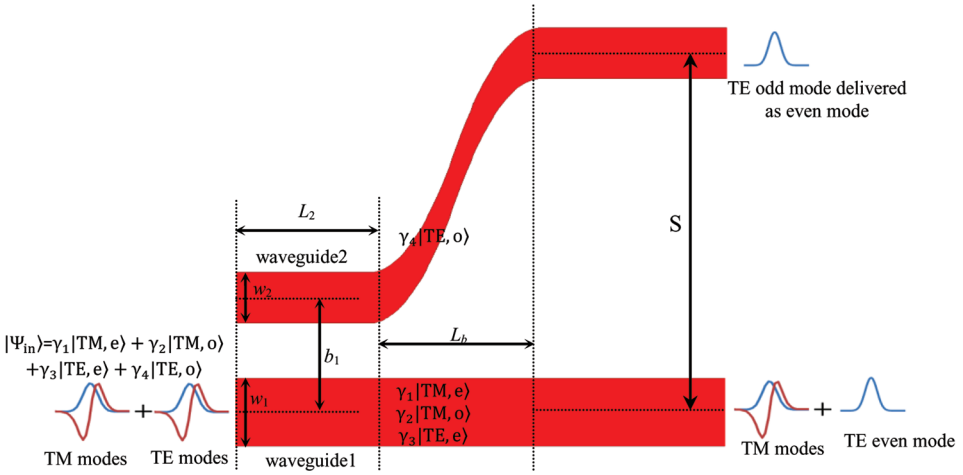

Figure 4. Sketch of a photonic circuit that serves as polarization-dependent mode analyzer (not to scale). TE and TM even and odd mode pathways are shown in this diagram. The TE odd mode is separated and delivered as an even mode. Dimensions of the device are $w_1 = 6.1$ μm, $w_2 = 3.4$ μm, $L_2 = 4.87$ mm, and $b_1 = 8.6$ μm. (color figure available online)

separation distance b_1 from the waveguide w_1 has been used to extract only the odd component of the TE-polarized input state. For this reason, $w_1 = 6.1$ μm and $w_2 = 3.4$ μm have been chosen, because in this case, the propagation constant of the TE odd mode in w_1 is equal to the TE even mode in w_2, as is specified in Figure 2. Thus, power can be coupled between these two modes and considering that $L_2 = 4.87$ mm and $b_1 = 8.6$ μm mode analyzer can separate them, deliver the TE odd mode as an even distribution, as shown in Figure 4. Note that according to [23], $b_1 < 8.25$ μm is experimentally not suitable because titanium diffusion to the surface will lead to partial fusion of two channels. b_1 has been chosen to be 8.6 μm to complete the exchange of TE odd mode power between w_1 and w_2. The end of the waveguide 2 is attached to an S-bend waveguide with standard spatial separation $S = 127$ μm and optimal length $L_b = 10$ mm [23] to obviate the possibility of further unwanted coupling to waveguide 1 and to provide a well-separated output port for the extracted mode.

Figure 5a shows the propagation of guided modes amplitude in the polarization-dependent mode analyzer when its input is a TE odd mode, and Figure 5b presents the normalized power amplitude of guided modes in the device. The amplitude of the even excited mode in waveguide 2 exhibits a dip that is associated with the tapered nature of the S-bend.

For TM-polarized light, the propagation constants in two waveguides of widths $w_1 = 6.1$ μm and $w_2 = 3.4$ μm are not matched; therefore, an exchange of power between waveguides cannot be complete. But interaction length L_2 has been adjusted such that the TM-polarized odd mode completely remains in waveguide 1. Figure 6a shows the propagation of guided-modes amplitude in the polarization-dependent mode analyzer when its input is a TM odd mode. Figure 6b presents the normalized power amplitude of guided modes in the device. The results have been obtained by using the commercial photonic and network design software package RSoft (RSoft Design Group, Inc., Ossining, New York, USA).

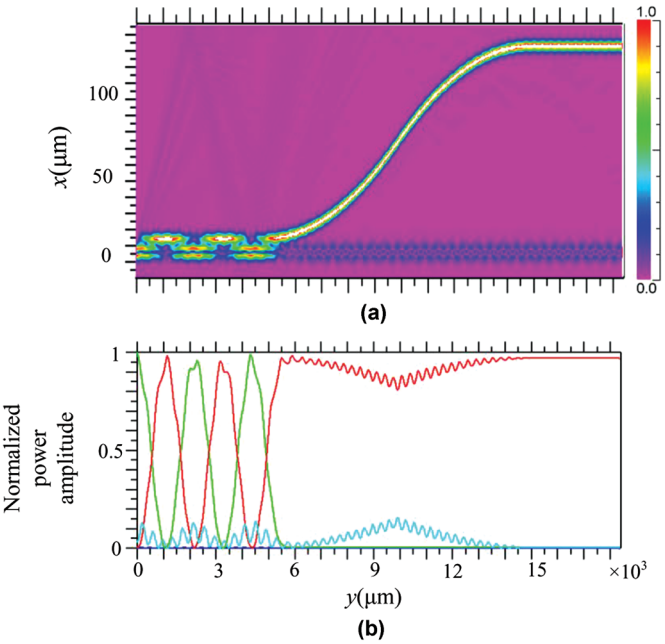

Figure 5. (a) Propagation of guided-modes amplitude in the polarization-dependent mode analyzer when its input is a TE odd mode. (b) The green curve represents the power evolution with distance of the TE odd mode in waveguide 1, and the red and cyan curves are related to TE even and odd modes, respectively, in waveguide 2. The dip in the curves is the result of the tapered nature of the S-bend. (color figure available online)

5. CZ Gate

Deterministic quantum computation that involves several degrees of freedom of a single photon for encoding multiple qubits is not scalable because it requires resources that grow exponentially [24]. A novel deterministic, two-qubit, single-photon, CZ gate implemented by Ti:$LiNbO_3$ photonic quantum circuit is proposed here. In this device, polarization of the photon has been used as a control qubit such that $|TM\rangle = |0\rangle$ and $|TE\rangle = |1\rangle$, and the mode number of photon as target qubit is $|e\rangle = |0\rangle$ and $|o\rangle = |1\rangle$. In general, when the control and target qubits are both in the superposition state, the quantum state of input $|\Psi_{in}\rangle$ is expressed as the tensor product of two superposition states as

$$|\Psi_{in}\rangle = (\alpha_1|TM\rangle + \alpha_2|TE\rangle) \otimes (\beta_1|e\rangle + \beta_2|o\rangle) = \gamma_1|TM, e|\rangle + \gamma_2|TM, o\rangle + \gamma_3|TE, e\rangle + \gamma_4|TE, o\rangle, \tag{10}$$

where α and β represent the basis weights; $\gamma_1 = \alpha_1\beta_1$, $\gamma_2 = \alpha_1\beta_2$, $\gamma_3 = \alpha_2\beta_1$, and $\gamma_4 = \alpha_2\beta_2$; and $\otimes$ indicates the tensor product. Since the target (modal) qubit is flipped by a TE control qubit, the output state of CZ gate becomes

$$|\Psi_{out}\rangle = \gamma_1|TM, e\rangle + \gamma_2|TM, o\rangle + \gamma_3|TE, e\rangle - \gamma_r|TE, o\rangle. \tag{11}$$

It can be seen in what follows how the designed structure can be used for implementation of Eq. (11). As established in Eq. (5), perfect coupling between a pair of adjacent

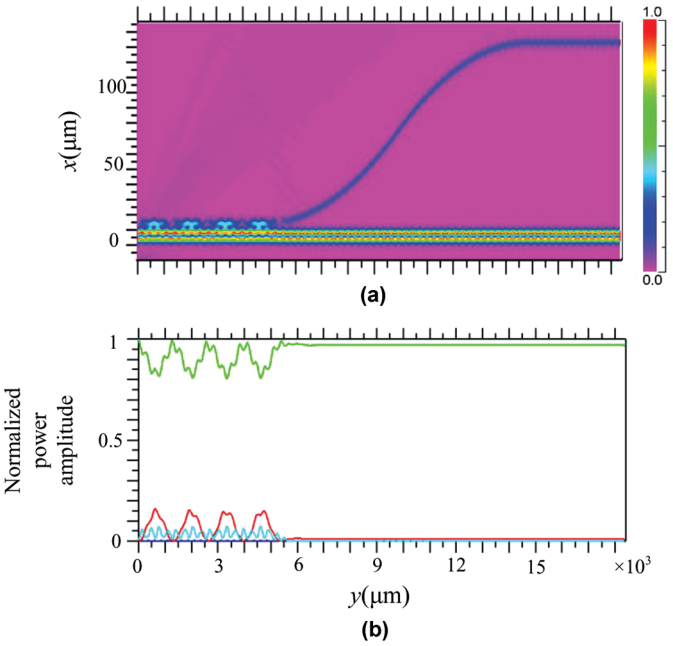

Figure 6. (a) Propagation of guided modes amplitude in the polarization-dependent mode analyzer when its input is a TM odd mode. (b) The green curve represents the power evolution with distance of the TM odd mode in waveguide 1, and the red and cyan curves are related to TM even and odd modes, respectively, in waveguide 2. (color figure available online)

waveguides over an interaction length $L = q\pi/2\kappa$ introduces a phase shift of $q\pi/2$, where q is an odd positive integer. A cascade of two such couplings thus results in a phase shift $q\pi$. Since the mode analyzer in Figure 4 has been designed so that perfect coupling can only occur for the TE-polarized odd component, a $q\pi$ phase shift for this component in interaction length $L = 2(\frac{q\pi}{2\kappa})$ can be expected. Thus, by cascading a polarization-dependent mode analyzer and a mode combiner (can be seen in Figure 7) and an appropriate adjustment of length L_3, a device can be obtained that introduces a π phase shift to the odd component of the TE-polarized input state while leaving other components of the input state (i.e., TE-polarized even or TM-polarized even and odd modes), unchanged.

By making use of EO phase modulators V_1 and V_2 in waveguides 1 and 2, respectively (as shown in Figure 7), imperfection in fabrication can be compensated for or the undesired phase shift of corresponding modes can be partially modified.

Figures 8 and 9 show the propagation of the normalized power of guided modes in a CZ gate when its input is a TE and TM odd mode, respectively. Figure 10 shows the real and imaginary part of CZ gate outputs when its inputs are TE and TM even and odd modes. As expected, TM even and odd modes remain almost unchanged, as well as the TE even mode while the TE odd mode undergoes a π phase shift.

Getting a more accurate output for the TM odd mode (ideally imaginary part must be zero) than that shown in Figure 10b may not be possible in this structure, because modifying V_2 will also change TE and TM even modes. The structure shown in Figure 11 is proposed for solving this problem. In this structure, the TM odd mode goes through

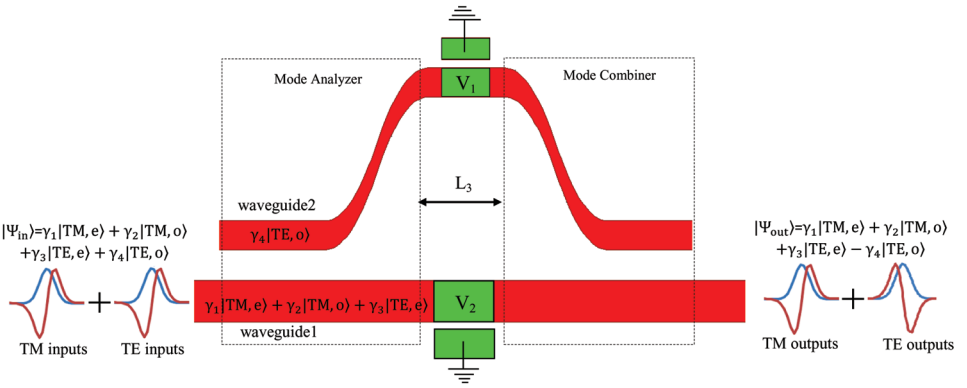

Figure 7. Sketch of a photonic circuit that serves as a CZ gate (not to scale). TE and TM even and odd modes path ways are shown in this diagram; $L_3 = 3.5$ mm. (color figure available online)

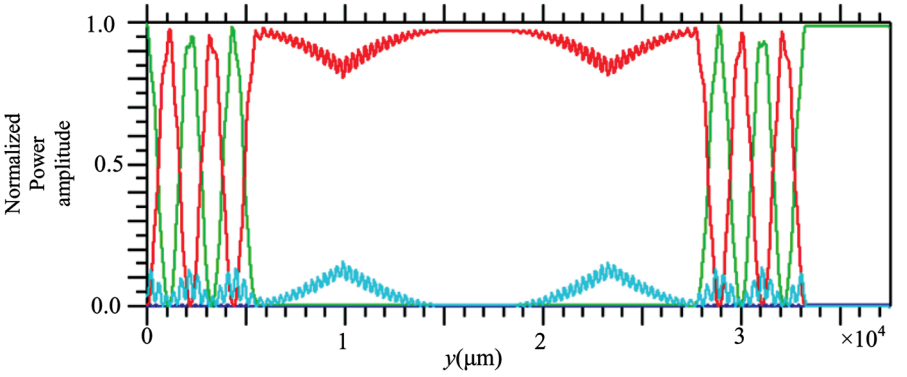

Figure 8. Propagation of normalized power in CZ gate when its input is a TE odd mode. The green curve represents the power evolution with distance of the TE odd mode in waveguide 1, and the red and cyan curves are related to TE even and odd modes, respectively, in waveguide 2. (color figure available online)

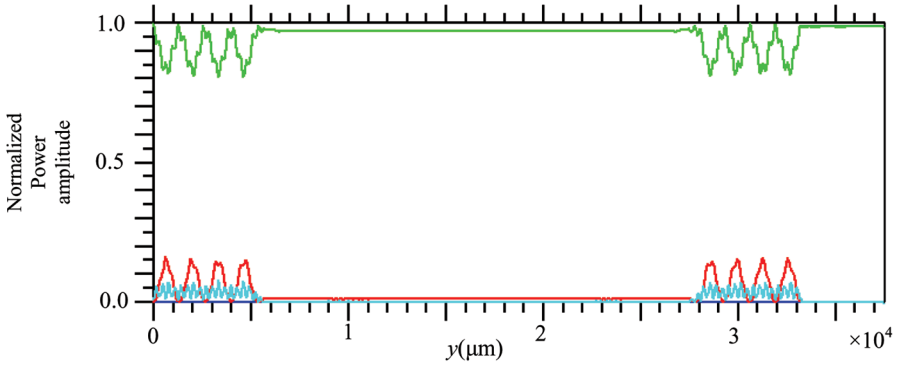

Figure 9. Propagation of normalized power in CZ gate when its input is a TM odd mode. The green curve represents the power evolution with distance of the TM odd mode in waveguide 1, and the red and cyan curves are related to TM even and odd modes, respectively, in waveguide 2. (color figure available online)

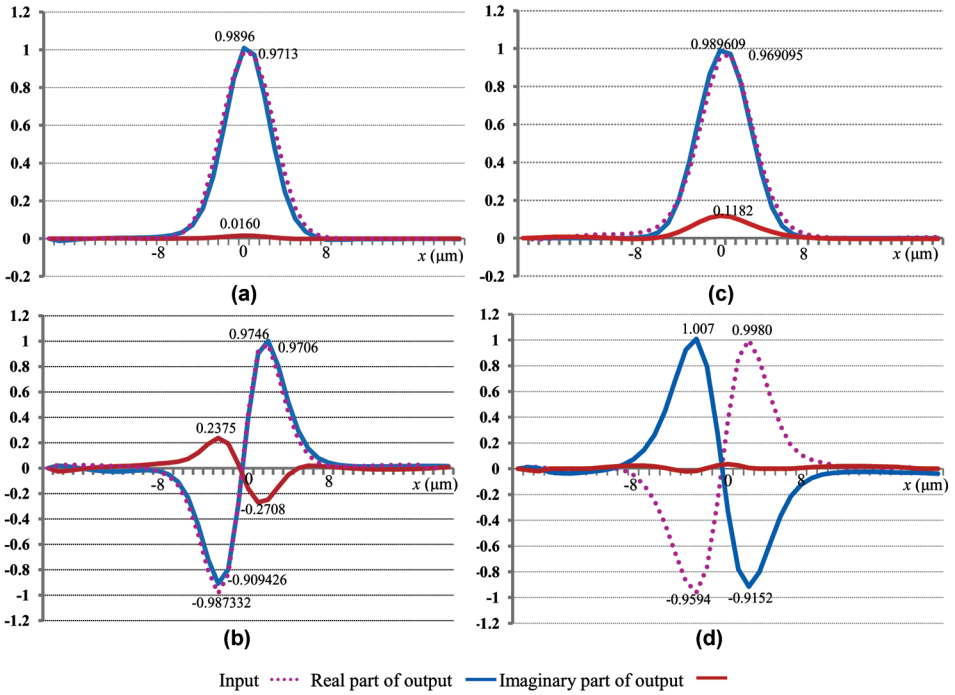

Figure 10. Real and imaginary parts of CZ gate output when its input is: (a) TM even mode: $|TM, e\rangle$, (b) TM odd mode: $|TM, o\rangle$, (c) TE even mode: $|TE, e\rangle$, and (d) TE odd mode: $|TE, o\rangle$. (color figure available online)

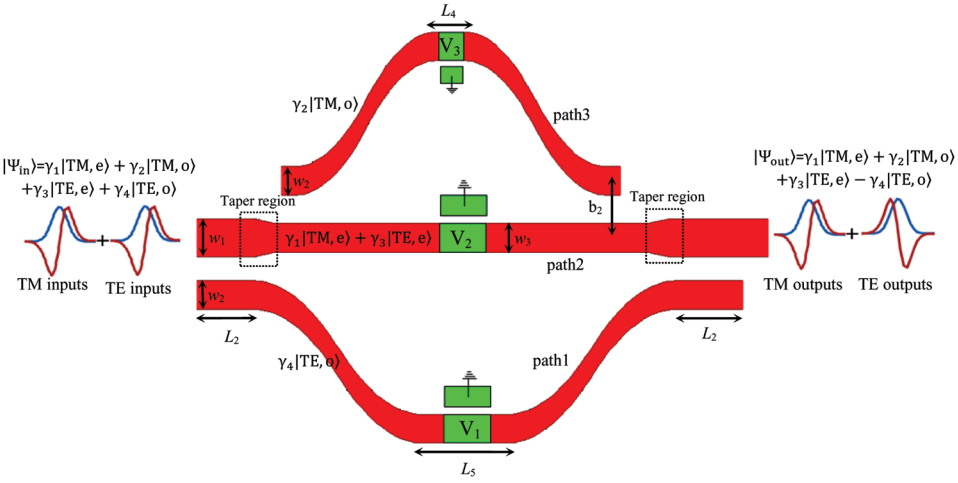

Figure 11. Sketch of the modified quantum photonic CZ gate (not to scale). TE and TM even and odd modes pathways are shown in this diagram; $w_1 = 6.1$ μm, $w_2 = 3.4$ μm, $w_3 = 5.6$ μm, $b_2 = 8.2$ μm, $L_2 = 4.87$ mm, $L_4 = 500$ μm, and $L_5 = 10$ mm. (color figure available online)

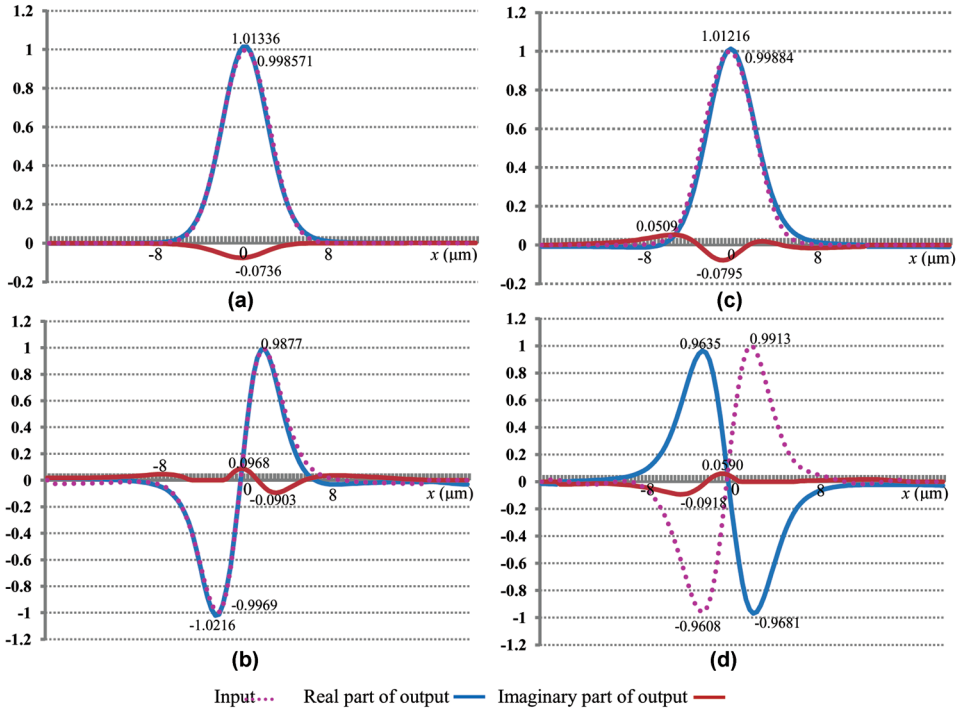

Figure 12. Real and imaginary parts of CZ gate output when its input is: (a) TM even mode: $|TM, e\rangle$, (b) TM odd mode: $|TM, o\rangle$, (c) TE even mode: $|TE, e\rangle$, and (d) TE odd mode: $|TE, o\rangle$. (color figure available online)

path 3. It is thus possible to control the TM odd mode independently through adjusting L_4 and V_3. For perfect coupling of the TM odd mode between waveguides 3 and 4, $w_3 = 3.4$ μm and $w_4 = 5.6$ μm have been chosen, as can be verified in Figure 3. A linear tapered region connects $w_1 = 6.1$ μm to $w_4 = 5.6$ μm. Figure 12 presents the real and imaginary parts of CZ gate outputs when its inputs are TE and TM even and odd modes. Comparing Figures 10b and 12b, it can be seen that the undesirable phase change of the output is omitted. A3D beam propagation method (BPM) simulation of the CZ gate shows that the propagation loss due to the device structure is well below 0.25 dB for both TE- and TM-polarization inputs.

6. Conclusions

This article presented a polarization-dependent mode analyzer based on Ti-diffusion waveguides, which separates the even and odd components of the TE-polarization incoming state into two separate spatial paths while TM-polarization even and odd modes remain unchanged. Based on this device, a 40-mm-long, 260-μm-wide deterministic two-qubit CZ quantum gate acting on the polarization and modal degrees of freedom of photons was designed. The gate performance relies on the selective coupling between two adjacent waveguides of different widths and polarization sensitivities of the Pockels coefficients in $LiNbO_3$. Its simple structure and short length, compared to other previous photonic quantum two-qubit gates [7], can greatly reduce propagation losses and

fabrication difficulties. Simulations of these devices, carried out with the help of the commercial photonic and network design software package RSoft, provide support that they operate as intended.

References

1. Ladd, T. D., Jelezko, F., Laflamme, R., Nakamura, Y., Monroe, C., and O'Brien, J. L. 2010. Quantum Computers. *Nature* 464(7285):45–53.
2. O'Brien, J. L., Furusawa, A., and Vuckovic, J. 2009. Photonic quantum technologies. *Nature Photonics* 687(3):687–695.
3. Kok, P., Munro, W. J., Nemoto, K., Ralph, T. C., Dowling, J. P., and Milburn, G. J. 2007. Linear optical quantum computing with photonic qubits. *Reviews of Modern Physics* 79(1):135–174.
4. Ursin, R., Tiefenbacher, F., Schmitt-Manderbach, T., Weier, H., Scheidl, T., Lindenthai, M., Blauensteiner, B., Jennewein, T., Perdigues, J., Trojek, P., Ömer, B., Furst, M., Meyenburg, M., Rarity, J., Sodnik, Z., Barbieri, C., Weinfurter, H., and Zeilinger, A. 2007. Entanglement-based quantum communication over 144 km. *Nature Physics* 3:481–486.
5. Crespi, A., Ramponi, R., Osellame, R., Sansoni, L., Bongioanni, I., Sciarrino, F., Vallone, G., and Mataloni, P. 2011. Integrated photonics quantum gates for polarization qubits. *Nature Communication* 2:1–6.
6. Salemian, S., and Mohammadnejad, S. 2011. An error-free protocol for quantum entanglement distribution in long-distance quantum communication. *Chinese Science Bulletin* 56(7):618–625.
7. Saleh, M. F., Di Giuseppe, G., Saleh, B. E. A., and Teich, M. C. 2010. Modal and polarization qubits in Ti:$LiNbO_3$ photonic circuits for a universal quantum logic gate. *Optics Express* 18:20475–20490.
8. Saleh, M. F., Di Giuseppe, G., Saleh, B. E. A., and Teich, M. C. 2010. Photonic circuits for generating modal, spectral, and polarization entanglement. *IEEE Photonics Journal* 2:736–752.
9. Saleh, M. F., Di Giuseppe, G., Saleh, B. E. A., and Teich, M. C. 2009. Modal, spectral, and polarization entanglement in guided-wave parametric down-conversion. *Physical Review A* 79:53842–53852.
10. Saleh, B. E. A, and Teich, M. C. 2007. *Fundamentals of Photonics*, 2nd ed. Hoboken, NJ: Wiley.
11. Busacca, A. C., Sones, C. L., Eason, R. W., and Mailis, S. 2004. First-order quasi-phase-matched blue light generation in surface-poled Ti:indiffused lithium niobate waveguides. *Applied Physics Letters* 84:4430–4432.
12. Armenise, M. N. 1988. Fabrication techniques of lithium niobate waveguides. *IEEE Proceedings* 135J(2):85–91.
13. Lee, Y. L., Jung, C., Noh, Y. C., Park, M., Byeon, C., Ko, D.-K., and Lee, J. 2004. Channel-selective wavelength conversion and tuning in periodically poled Ti:$LiNbO_3$ waveguides. *Optics Express* 12:2649–2655.
14. McMahon, D. 2008. Quantum gates and circuits. In: *Quantum Computing Explained*. John Wiley & Sons.
15. Langford, N. K., Weinhold, T. J., Prevedel, R., Resch, K. J., Gilchrist, A., O'Brien, J. L., Pryde, G. J., and White, A. G. 2005. Demonstration of a simple entangling optical gate and its use in Bell-state analysis. *Physical Review Letters* 95:210504.
16. Menicucci, N. C., van Loock, P., Gu, M., Weed-brook, C., Ralph, T. C., and Nielsen, M. A. 2006. Universal quantum computation with continuous-variable cluster states. *Physical Review Letters* 97(11):110501.
17. Wang, M., Jiang, N., Jin, Q., and Zheng, Y. 2011. Continuous-variable controlled-Z gate using an atomic ensemble. *Physical Review Letters A* 83:062339.
18. Abernethy, J. A. 2003. *Novel devices in periodically poled lithium niobate*. Doctoral Thesis, University of Southampton, Southampton, UK.
19. Jundt, D. H.1997. Temperature-dependent Sellmeier equation for the index of refraction, n_e, in congruent lithium niobate. *Optics Letters* 22:1553–1555.

20. Wong, K. K., ed. 2002. *Properties of Lithium Niobate*. Stevenage, U.K.: Institution of Electrical Engineers.
21. Nielsen, M. A., and Chuang, I. L. 2000. *Quantum Computation and Quantum Information.* Cambridge University Press.
22. Barenco, A., Bennett, C. H., Cleve, R., DiVincenzo, D. P., Margolus, N., Shor, P., Sleator, T., Smolin, J., and Weinfurter, H. 1995. Elementary gates for quantum computation. *Physical Review A* 52:3457–3467.
23. Runde, D., Breuer, S., and Kip, D. 2008. Mode-selective coupler for wavelength multiplexing using Ti:$LiNbO_3$ optical waveguide. *Central European Journal of Physics* 6(3):588–592.
24. Fiorentino, M., and Wong, F. N. C. 2004. Deterministic controlled-NOT gate for single-photon two-qubit quantum logic. *Physical Review Letters* 93(7):070502.

Biographies

Masoomeh Taherkhani was born in Takestan, Iran, in 1983. She received her M.Sc. in electronics engineering in 2009, and she is currently pursuing her Ph.D. at Nanoptronics Research Center, Iran, University of Science and Technology (IUST), Tehran, Iran. Her research interests are quantum electronics and photonics.

Shahram Mohammad Nejad received his B.Sc. in electrical engineering from the University of Houston, Houston, TX, in 1981, and his M.Sc. and Ph.D. in semiconductor material growth and lasers from Shizuoka University, Shizuoka, Japan, in 1990 and 1993, respectively. He invented the PbSrS laser in 1992. He has published more than 200 scientific papers and books. His research interests include semiconductor material growth, quantum electronics, semiconductor devices, optoelectronics, nanoelectronics, and lasers. He is a scientific committee member of the Iranian Conference of Electrical Engineering (ICEE) and Photonics, a member of the Institute of Engineering and Technology (IET), and a member of IET-CEng. He has been the director of *IJEEE Journal* of the Iran University of Science and Technology (IUST) for several years and is also an editorial board member for several international scientific magazines. He is currently an active professor at IUST and has established and is directing the Nanoptronics Research center at IUST.